10.1098/rspa.2003.1273

On two-phase sediment transport: sheet flow of massive particles

By Tian-Jian Hsu[1]†, James T. Jenkins[2] and Philip L.-F. Liu[1]

[1] *School of Civil and Environmental Engineering and*
[2] *Department of Theoretical and Applied Mechanics,*
Cornell University, Ithaca, NY 14853, USA
(thsu@whoi.edu)

Received 13 January 2003; revised 15 October 2003; accepted 26 November 2003; published online 5 May 2004

A model is presented for concentrated sediment transport that is driven by strong, fully developed turbulent shear flows over a mobile bed. Balance equations for the average mass, momentum and energy for the two phases are phrased in terms of concentration-weighted (Favre averaged) velocities. Closures for the correlations between fluctuations in concentration and particle velocities are based on those for collisional grain flow. This is appropriate for particles that are so massive that their fall velocity exceeds the friction velocity of the turbulent fluid flow. Particular attention is given to the slow flow in the region of high concentration above the stationary bed. A failure criterion is introduced to determine the location of the stationary bed. The proposed model is solved numerically with a finite-difference algorithm in both steady and unsteady conditions. The predictions of sediment concentration and velocity are tested against experimental measurements that involve massive particles. The model is further employed to study several global features of sheet flow such as the total sediment transport rate in steady and unsteady conditions.

Keywords: sediment transport; sheet flow; particle collisions; turbulent suspension; two-phase flow

1. Introduction

Sheet flows occur when the shear stress of a turbulent fluid flow is large enough that bed ripples disappear and a significant amount of highly concentrated sediment is suspended and transported. Within the sheet, particles interact with each other, with the bed and with the turbulent shear flow. Sheet flows are important because a relatively large amount of sediment can be transported within them. Also, it is likely that they exhibit, in expanded form, the structure of thinner regions of bedload in milder conditions. That is, high concentration and collisional suspension near the bed, with turbulent suspension becoming increasingly important as the strength of the turbulence increases with distance from the bed and the concentration decreases.

† Present address: Applied Ocean Physics and Engineering Department, Woods Hole Oceanographic Institution, Woods Hole, MA 02543, USA.

The most important elements in the modelling of sheet flows are the implementation of the appropriate governing equations for the sediment dynamics, including closures for the intergranular stresses, and an accurate description of the influence of particles on fluid turbulence. In the simplest models of sheet flow (see, for example, Hanes & Bowen 1985; Wilson 1987), the sediment concentration profile is not a solution of the governing equations and is specified in advance; also, Bagnold's (1954) quadratic stress relations are employed for the closure of particle stress. More complicated models of sheet flow employ two-phase mass and momentum equations in which the sediment concentration and velocity are described by an independent set of balance equations (see, for example, Kobayashi & Seo 1985; Asano 1990; Dong & Zhang 1999; Greimann & Holly 2001). In this event, the sediment concentration profile is a part of the solution of the two-phase equations. However, the closure of particle stress in most of these models is still based on Bagnold's stress relations, obtained in a simple shear flow. In sediment transport, the flow is inevitably inhomogeneous and such simple relations are not necessarily valid.

Jenkins & Hanes (1998) also studied sheet-flow based on two-phase equations. To close the particle stress, they introduced the granular temperature, a measure of the strength of the particle velocity fluctuations. For particles whose inertia is large compared with the viscous resistance of the fluid (Bagnold 1954), transport processes are dominated by collisions between particles. The granular temperature and the particle stresses may be calculated using a modification of the kinetic theory appropriate for dense, inelastic spheres (Jenkins & Savage 1983). That is, the granular temperature may be calculated from a balance equation, and the particle pressure and the particle viscosity are given in terms of granular temperature by the kinetic theory.

In the upper portion of a sheet, the suspension of sediment is mainly due to the velocity fluctuations of the fluid. In Jenkins & Hanes (1998), turbulent suspension is ignored in the momentum balance. Recently, Hsu *et al.* (2003) examined both the importance of turbulent suspension in sediment transport and the impact of sediment on fluid turbulence. They carry out a second average, phrased in terms of concentration-weighted (Favre averaged) velocities, on the two-phase equations of Drew (1983) and introduce turbulence closures for the resulting correlations. In dilute flows, they ignore the stresses in the sediment phase and test the model against experiments on sediment transport in open channel flow.

Within the stationary sediment bed, it is likely that sediment particles are random close packed. In this region, both the mean and fluctuating motions of particles vanish, but the fluid can still flow thorough pores. Near the top of the stationary bed, the bed begins to fail and is fluidized by the flow. In the region where the concentration is between random close packing and random loose packing (see, for example, Onoda & Liniger 1990), the particles are in a transitional condition between the solid-like and fluid-like behaviour (see, for example, Zhang & Campbell 1992). In this region, the mean motion of the sediment is almost negligible, but the fluctuations of the particles can still be important. Moreover, due to the high concentration, part of the particle stress in this region is supported by enduring contact, rather than collisions. Jenkins & Hanes (1998) avoid solving for the sediment motion in this region by defining their 'bottom boundary' to be at a specified concentration, where the fluid and sediment velocity are assumed to be zero. They prescribe the flux of the granular temperature at this boundary using the results of a theoretical study by Jenkins & Askari (1991).

In this paper, we continue the work of Jenkins & Hanes (1998) and Hsu *et al.* (2003). The two-phase equations of Hsu *et al.* (2003) are first summarized. A closure model for particle stresses, based on the fluctuation energy of the sediment-phase, similar to that of Jenkins & Hanes (1998), is then introduced. However, an attempt is also made to model the sediment transport in the transitional region above the porous stationary bed. This is done by modifying the closure of Jenkins & Hanes (1998) for the shear stress using a viscosity appropriate to a glassy solid (Bocquet *et al.* 2001) and by introducing a closure for particle pressure due to enduring contact (Jenkins *et al.* 1989). The Coulomb failure criterion is employed in order to determine the location of the stationary bed. The resulting system of partial differential equations and boundary conditions is solved numerically using a finite-difference scheme. The predictions are tested against the results of sheet flow experiments using relatively massive particles carried out on steady, fully developed flows by Sumer *et al.* (1996) and on oscillatory flows by Asano (1995). Further results based on the present model on several global features of sheet flow are also presented.

2. Model formulation

(*a*) *Two-phase equations for sediment transport*

Sediment transport involves a fluid phase and a particle phase. The fluid phase is water with mass density ρ^{f} and the particle phase is taken to be identical spheres of diameter d and mass density ρ^{s}. Assuming that the mixture can be treated as a continuum, the ensemble averaged two-phase equations of mass and momentum can be derived readily (Drew 1983). In this averaging process, the definition of sediment concentration c is introduced. Because of the flow turbulence, this sediment concentration fluctuates on a scale much larger than the grain size. Therefore, a second averaging process needs to be carried out in order to calculate the large scale turbulence. Because of the presence of the particle concentration, the two continuum phases are, essentially, compressible. For this reason, we implement Favre averaging (Favre 1965). In this paper, only the final equations obtained after the Favre averaging are presented. The details of the derivations of the equations are given by Drew (1983) and Hsu *et al.* (2003).

We consider the closure of these equations for sheet flow in uniform conditions, either steady or oscillatory. The steady flow is that driven by gravity in a channel with small inclination angle ξ and uniform water depth h. The oscillatory flow is that in a U-tube.

When the flow is uniform in the x-direction, the fluid and sediment phase continuity equations are (Hsu *et al.* 2003)

$$\frac{\partial \rho^{\mathrm{f}}(1-\bar{c})}{\partial t} + \frac{\partial \rho^{\mathrm{f}}(1-\bar{c})\tilde{w}^{\mathrm{f}}}{\partial z} = 0 \tag{2.1}$$

and

$$\frac{\partial \rho^{\mathrm{s}}\bar{c}}{\partial t} + \frac{\partial \rho^{\mathrm{s}}\bar{c}\tilde{w}^{\mathrm{s}}}{\partial z} = 0, \tag{2.2}$$

where z is normal to the channel bottom and $\tilde{w}^{\mathrm{f}}$ and $\tilde{w}^{\mathrm{s}}$ are, respectively, the z-components of the fluid and particle average velocity.

The x- and z-components of the fluid-phase momentum equations for the uniform flow can be expressed as

$$\frac{\partial \rho^{\mathrm{f}}(1-\bar{c})\tilde{u}^{\mathrm{f}}}{\partial t} = -\frac{\partial \rho^{\mathrm{f}}(1-\bar{c})\tilde{u}^{\mathrm{f}}\tilde{w}^{\mathrm{f}}}{\partial z} - (1-\bar{c})\frac{\partial \bar{P}^{\mathrm{f}}}{\partial x} + \frac{\partial \tau^{\mathrm{f}}_{xz}}{\partial z} - \rho^{\mathrm{f}}(1-\bar{c})Sg - \beta\bar{c}(\tilde{u}^{\mathrm{f}} - \tilde{u}^{\mathrm{s}}) \tag{2.3}$$

and

$$\frac{\partial \rho^{\mathrm{f}}(1-\bar{c})\tilde{w}^{\mathrm{f}}}{\partial t} = -\frac{\partial \rho^{\mathrm{f}}(1-\bar{c})\tilde{w}^{\mathrm{f}}\tilde{w}^{\mathrm{f}}}{\partial z} - (1-\bar{c})\frac{\partial \bar{P}^{\mathrm{f}}}{\partial z} + \frac{\partial \tau^{\mathrm{f}}_{zz}}{\partial z} + \rho^{\mathrm{f}}(1-\bar{c})g - \beta\bar{c}(\tilde{w}^{\mathrm{f}} - \tilde{w}^{\mathrm{s}}) + \beta\nu_{\mathrm{ft}}\frac{\partial \bar{c}}{\partial z}, \tag{2.4}$$

where $\tilde{u}^{\mathrm{f}}$ and $\tilde{u}^{\mathrm{s}}$ are, respectively, the x-components of the fluid and particle average velocity, $\bar{P}^{\mathrm{f}}$ is the average fluid pressure, $S \equiv \sin\xi \doteq \xi$ for channel flows, τ^{f}_{xz} and τ^{f}_{zz} are fluid phase stresses, including the fluid viscous stress and both the small-scale and large-scale fluid Reynolds stresses, and $g = -9.8\ \mathrm{m\,s^{-2}}$ is the gravitational acceleration. The last two terms in equation (2.4) are the Favre averaged drag force, with the drag coefficient β defined as

$$\beta = \frac{\rho^{\mathrm{f}}U_{\mathrm{r}}}{d}\left(\frac{18.0}{Re_{\mathrm{p}}} + 0.3\right)\frac{1}{(1-\bar{c})^{n}}, \tag{2.5}$$

in which

$$U_{\mathrm{r}} = \sqrt{(\tilde{u}^{\mathrm{f}} - \tilde{u}^{\mathrm{s}})^2 + (\tilde{w}^{\mathrm{f}} - \tilde{w}^{\mathrm{s}})^2} \tag{2.6}$$

is the magnitude of the relative velocity between the fluid and sediment phase. Hence, the particle Reynolds number Re_{p} is defined as

$$Re_{\mathrm{p}} = \frac{\rho^{\mathrm{f}}U_{\mathrm{r}}d}{\mu_{\mathrm{f}}}, \tag{2.7}$$

with μ_{f} the fluid viscosity. The concentration dependence in equation (2.5) is taken from the experimental results of Richardson & Zaki (1954), with n a coefficient depending on the particle Reynolds number,

$$n = 4.45Re_{\mathrm{p}}^{-1}, \quad 1 \leqslant Re_{\mathrm{p}} < 500.$$

The drag force contributes two terms in (2.4). The first is the averaged drag force due to the relative mean velocity between two phases. The second, called fluid turbulent suspension, is obtained in the Favre averaging and is the correlation $\overline{c\Delta u^{\mathrm{f}}_i}$ between the concentration and the large-scale fluid velocity fluctuations. It is modelled here as a gradient transport (see, for example, McTigue 1981).

The corresponding sediment-phase momentum equations are

$$\frac{\partial \rho^{\mathrm{s}}\bar{c}\tilde{u}^{\mathrm{s}}}{\partial t} = -\frac{\partial \rho^{\mathrm{s}}\bar{c}\tilde{u}^{\mathrm{s}}\tilde{w}^{\mathrm{s}}}{\partial z} - \bar{c}\frac{\partial \bar{P}^{\mathrm{f}}}{\partial x} + \frac{\partial \tau^{\mathrm{s}}_{xz}}{\partial z} - \rho^{\mathrm{s}}\bar{c}Sg + \beta\bar{c}(\tilde{u}^{\mathrm{f}} - \tilde{u}^{\mathrm{s}}) \tag{2.8}$$

and

$$\frac{\partial \rho^{\mathrm{s}}\bar{c}\tilde{w}^{\mathrm{s}}}{\partial t} = -\frac{\partial \rho^{\mathrm{s}}\bar{c}\tilde{w}^{\mathrm{s}}\tilde{w}^{\mathrm{s}}}{\partial z} - \bar{c}\frac{\partial \bar{P}^{\mathrm{f}}}{\partial z} + \frac{\partial \tau^{\mathrm{s}}_{zz}}{\partial z} + \rho^{\mathrm{s}}\bar{c}g + \beta\bar{c}(\tilde{w}^{\mathrm{f}} - \tilde{w}^{\mathrm{s}}) - \beta\nu_{\mathrm{ft}}\frac{\partial \bar{c}}{\partial z}, \tag{2.9}$$

where τ_{xz}^{s} and τ_{zz}^{s} are the stresses of the sediment phase, including the small-scale particle (intergranular) stresses and the Reynolds stresses of the Favre averaged particle velocities. Closures for fluid turbulence and sediment stresses are major foci of sheet flow modelling and are detailed in the next few sections.

(*b*) *Closures of fluid stresses*

The total stress of the fluid-phase in equations (2.3) and (2.4) can be written as

$$\tau_{xz}^{\mathrm{f}} = \tau_{xz}^{\mathrm{f0}} + R_{xz}^{\mathrm{f}} \quad \text{and} \quad \tau_{zz}^{\mathrm{f}} = \tau_{zz}^{\mathrm{f0}} + R_{zz}^{\mathrm{f}}, \tag{2.10}$$

where τ_{xz}^{f0} and τ_{zz}^{f0} are the averaged small-scale stresses consisting of the viscous stress and the small-scale Reynolds stress of the turbulence generated in the fluid between the sediment particles or induced by fluctuations of the particles. The large-scale fluid Reynolds stresses, defined as the correlations between the concentration and fluid velocity fluctuations Δu^{f} and Δw^{f},

$$R_{xz}^{\mathrm{f}} = -\rho^{\mathrm{f}}\,\overline{(1-c)\Delta u^{\mathrm{f}}\Delta w^{\mathrm{f}}} \quad \text{and} \quad R_{zz}^{\mathrm{f}} = -\rho^{\mathrm{f}}\,\overline{(1-c)\Delta w^{\mathrm{f}}\Delta w^{\mathrm{f}}}, \tag{2.11}$$

result from the Favre averaging process. They represent the transfer of momentum that occurs on the scale at which the concentration fluctuates.

The turbulent eddy viscosity hypothesis is used here to model the large-scale fluid Reynolds stresses:

$$\tau_{xz}^{\mathrm{f}} = \rho^{\mathrm{f}}(\nu_{\mathrm{ft}} + \nu_{\mathrm{f}})\frac{\partial \tilde{u}^{\mathrm{f}}}{\partial z} \tag{2.12}$$

and

$$\tau_{zz}^{\mathrm{f}} = -\tfrac{2}{3}\rho^{\mathrm{f}}(1-\bar{c})k_{\mathrm{f}} + \tfrac{4}{3}\rho^{\mathrm{f}}(\nu_{\mathrm{ft}} + \nu_{\mathrm{f}})\frac{\partial \tilde{w}^{\mathrm{f}}}{\partial z}, \tag{2.13}$$

where ν_{f} is the kinematic viscosity of the fluid and k_{f} is the fluid-phase turbulent kinetic energy, defined as

$$k_{\mathrm{f}} \equiv \frac{1}{2(1-\bar{c})}\overline{(1-c)\Delta u_i^{\mathrm{f}}\Delta u_i^{\mathrm{f}}}. \tag{2.14}$$

The second term on the right-hand side of equation (2.13) appears because the divergence of the fluid-phase velocity is not zero. We assume that the fluid phase eddy viscosity ν_{ft} is given by

$$\nu_{\mathrm{ft}} = C_\mu \frac{k_{\mathrm{f}}^2(1-\bar{c})}{\epsilon_{\mathrm{f}}}, \tag{2.15}$$

where C_μ is an empirical coefficient and

$$\epsilon_{\mathrm{f}} \equiv \frac{1}{\rho^{\mathrm{f}}(1-\bar{c})}\overline{(1-c)\tau_{ij}^{\mathrm{f}}\frac{\partial \Delta u_i^{\mathrm{f}}}{\partial x_j}} \tag{2.16}$$

is the fluid-phase turbulent dissipation rate. Because k_{f} and ϵ_{f} appear in the eddy viscosity, we need to introduce balance equations for both.

Table 1. *Summary of all numerical coefficients adopted by the model*

C_μ	$C_{\epsilon 1}$	$C_{\epsilon 2}$	$C_{\epsilon 3}$	σ_k	σ_ϵ	C_s	σ_s
0.09	1.44	1.92	1.2	1.0	1.3	0.55	1.0

Following Hsu *et al.* (2003), the fluid phase turbulent kinetic energy equation in the uniform flow can be written as

$$\begin{aligned}\frac{\partial \rho^\mathrm{f}(1-\bar{c})k_\mathrm{f}}{\partial t} &+ \frac{\partial \rho^\mathrm{f}(1-\bar{c})k_\mathrm{f}\tilde{w}^\mathrm{f}}{\partial z} \\ &= \tau_{xz}^{ft}\frac{\partial \tilde{u}^\mathrm{f}}{\partial z} + \tau_{zz}^{ft}\frac{\partial \tilde{w}^\mathrm{f}}{\partial z} + \frac{\partial}{\partial z}\left[\left(\nu + \frac{\nu_\mathrm{ft}}{\sigma_k}\right)\frac{\partial \rho^\mathrm{f}(1-\bar{c})k_\mathrm{f}}{\partial z}\right] - \rho^\mathrm{f}(1-\bar{c})\epsilon_\mathrm{f} \\ &\quad + \beta\nu_\mathrm{ft}\frac{\partial \bar{c}}{\partial z}(\tilde{w}^\mathrm{f} - \tilde{w}^\mathrm{s}) - 2\rho^\mathrm{s}\bar{c}\beta k_\mathrm{f}(1-\alpha). \end{aligned} \tag{2.17}$$

The last term in (2.17), which originally involve correlations between fluctuations of fluid and sediment velocities, represents a dissipation mechanism for the turbulent energy, where α is a parameter that measures the degree of correlation between the fluid and sediment velocity fluctuations. It is determined by the relative magnitudes of a particle response time t_p, the time between collisions t_c, and the fluid turbulence time-scale t_L:

$$\alpha \equiv \left(1 + \frac{t_\mathrm{p}}{\min(t_\mathrm{L}, t_\mathrm{c})}\right)^{-1}. \tag{2.18}$$

The particle response time is defined as

$$t_\mathrm{p} \equiv \frac{\rho^\mathrm{s}}{\beta}; \tag{2.19}$$

it is a measure of the time to accelerate a single particle from rest to the velocity of surrounding fluid (Drew 1976). The time between collisions is estimated based on the mean free path l_c of colliding particles and the strength $k_\mathrm{s}^{1/2}$ of sediment velocity fluctuations:

$$t_\mathrm{c} = \frac{l_\mathrm{c}}{k_\mathrm{s}^{1/2}}, \tag{2.20}$$

where

$$l_\mathrm{c} = \frac{\sqrt{\pi}d}{24\bar{c}g_0(\bar{c})} \tag{2.21}$$

and $g_0(\bar{c})$ is the contact value of the radial distribution function (see, for example, Chapman & Cowling 1970). The quantities k_s and $g_0(\bar{c})$ will be defined in the next section. The fluid turbulence time-scale is defined as (Elghobashi & Abou-Arab 1983)

$$t_\mathrm{L} \equiv 0.165\frac{k_\mathrm{f}}{\epsilon_\mathrm{f}}. \tag{2.22}$$

The rate of turbulent energy dissipation ϵ_f is assumed to be governed by an equation similar to that for a clear fluid (Elghobashi & Abou-Arab 1983):

$$\begin{aligned}\frac{\partial\rho^\mathrm{f}(1-\bar{c})\epsilon_\mathrm{f}}{\partial t}&+\frac{\partial\rho^\mathrm{f}(1-\bar{c})\epsilon_\mathrm{f}\tilde{w}^\mathrm{f}}{\partial z}\\&=C_{\epsilon1}\frac{\epsilon_\mathrm{f}}{k_\mathrm{f}}\left(\tau^{ft}_{xz}\frac{\partial\tilde{u}^\mathrm{f}}{\partial z}+\tau^{ft}_{zz}\frac{\partial\tilde{w}^\mathrm{f}}{\partial z}\right)\\&\quad+\frac{\partial}{\partial z}\left[\left(\nu+\frac{\nu_\mathrm{ft}}{\sigma_\epsilon}\right)\frac{\partial\rho^\mathrm{f}(1-\bar{c})\epsilon_\mathrm{f}}{\partial z}\right]-C_{\epsilon_2}\frac{\epsilon_\mathrm{f}}{k_\mathrm{f}}\rho^\mathrm{f}(1-\bar{c})\epsilon_\mathrm{f}\\&\quad-C_{\epsilon_3}\frac{\epsilon_\mathrm{f}}{k_\mathrm{f}}[2\rho^\mathrm{s}\bar{c}k_\mathrm{f}\beta(1-\alpha)]+C_{\epsilon_3}\frac{\epsilon_\mathrm{f}}{k_\mathrm{f}}\left[\beta\nu_\mathrm{ft}\frac{\partial\bar{c}}{\partial z}(\tilde{w}^\mathrm{f}-\tilde{w}^\mathrm{s})\right].\end{aligned}\tag{2.23}$$

Due to the lack of information regarding the appropriate values of numerical coefficients in the present $k_\mathrm{f}-\epsilon_\mathrm{f}$ model, we employ the same coefficients as those implemented in the standard $k-\epsilon$ model for a clear fluid flow (Rodi 1984). We adopt a numerical value of C_{ϵ_3} suggested by Elghobashi & Abou-Arab (1983) based on their research on sediment-laden jets. However, we find that C_{ϵ_3} is quite sensitive to the calculated flow velocities of the present model based on numerical experiments. A list of the numerical coefficients adopted by the present model is shown in table 1.

The small-scale fluid turbulence can be important for relatively large particles (see, for example, Gore & Crowe 1989). Although it does not directly contribute to the transport of sediment, it dissipates mean flow energy and thus influences the flow rate. Due to the lack of appropriate closures for the small-scale fluid turbulence in concentrated collisional flow, it is neglected here.

(*c*) *Closure of the sediment stress*

In the sediment momentum equations, the two-scale averaging process results in a sediment stress, which can be written as

$$\tau^\mathrm{s}_{xz}=\tau^\mathrm{s0}_{xz}+R^\mathrm{s}_{xz}\quad\text{and}\quad\tau^\mathrm{s}_{zz}=\tau^\mathrm{s0}_{zz}+R^\mathrm{s}_{zz},\tag{2.24}$$

where τ^s0_{xz} and τ^s0_{zz} are the mean particle shear and normal stress due to small scale interactions, while R^s_{xz} and R^s_{zz} are components of the large-scale sediment Reynolds stress,

$$R^\mathrm{s}_{xz}=-\rho^\mathrm{s}\,\overline{c\Delta u^\mathrm{s}\Delta w^\mathrm{s}}\quad\text{and}\quad R^\mathrm{s}_{zz}=-\rho^\mathrm{s}\,\overline{c\Delta w^\mathrm{s}\Delta w^\mathrm{s}},\tag{2.25}$$

given in terms of Δu^s and Δw^s, the large-scale sediment velocity fluctuations.

(i) *Sediment fluctuation energy equation*

In the closure of the small-scale particle stress, a measure of the strength of the small-scale particle velocity fluctuation, the granular temperature T_s, is usually introduced (Nott & Brady 1994; Jenkins & Hanes 1998):

$$T_\mathrm{s}=\tfrac{1}{3}\langle u^{\mathrm{s}\prime\prime}_i u^{\mathrm{s}\prime\prime}_i\rangle,\tag{2.26}$$

where '$\langle\cdot\rangle$' denotes the small-scale ensemble averaging operator and $u^{\mathrm{s}\prime\prime}_i$ the small-scale particle velocity fluctuations.

Similarly, we propose closures for the large-scale sediment stresses by introducing a measure of the strength of the large-scale sediment velocity fluctuations, represented by

$$k_{\mathrm{s}} \equiv \frac{1}{2\bar{c}}\overline{c\Delta u_i^{\mathrm{s}}\Delta u_i^{\mathrm{s}}}. \tag{2.27}$$

To solve for T_{s} and k_{s}, their corresponding transport equations are needed. The transport equation of the small-scale granular temperature T_{s} in a two-phase fluid–particle system has been derived by, for example, Hwang & Shen (1993). Likewise, the transport equation of the large-scale sediment fluctuation energy k_{s} can be derived from the sediment momentum equation (see, for example, Hsu 2002). Since both transport equations for T_{s} and k_{s} have similar terms (i.e. terms that represent unsteadiness, convection, diffusion, dissipation and interphase interactions) and require further closure assumptions, we adopt a single fluctuation energy, K_{s} to model both the small-scale and large-scale processes. The transport equation for K_{s} is taken to be (Hsu 2002)

$$\rho^{\mathrm{s}}\left(\frac{\partial \bar{c}K_{\mathrm{s}}}{\partial t} + \frac{\partial \bar{c}K_{\mathrm{s}}\tilde{w}^{\mathrm{s}}}{\partial z}\right) = \tau_{xz}^{\mathrm{s}}\frac{\partial \tilde{u}^{\mathrm{s}}}{\partial z} + \tau_{zz}^{\mathrm{s}}\frac{\partial \tilde{w}^{\mathrm{s}}}{\partial z} - \frac{\partial Q}{\partial z} - \gamma + 2\beta\bar{c}(\alpha k_{\mathrm{f}} - K_{\mathrm{s}}), \tag{2.28}$$

with Q the flux of the fluctuation energy and γ the dissipation. The last term in the above equation describes the interaction between the phases. Therefore, there is an additional source term, $2\beta\bar{c}\alpha k_{\mathrm{f}}$, due to the fluid turbulent kinetic energy. This term models the influence of fluid turbulent eddies on the random motions of sediment particles and permits turbulent eddies to enhance the sediment fluctuation energy. Moreover, an additional dissipation mechanism, $2\beta\bar{c}K_{\mathrm{s}}$, also appears due to the drag of the interstitial fluid.

In order to solve equation (2.28), further closure assumptions are needed for sediment stresses, flux of fluctuation energy and dissipation. We shall propose closures based on summation of processes resulted from both the small-scale and large-scale. This is somewhat justified because the small-scale and large-scale processes are assumed to be uncorrelated due to their difference in scale. Although our treatment of the sediment fluctuation energy and its transport equation is somewhat heuristic, it does include the known mechanisms of fluid–particle and particle–particle interactions in a plausible way and simplifies the model substantially.

The averaged small-scale stresses $\tau_{xz}^{\mathrm{s}0}$ and $\tau_{zz}^{\mathrm{s}0}$ are mainly due to intergranular interactions resulting from particle collisions or interstitial fluid effects. Here, we adopt the kinetic theory for collisional granular flow (Jenkins & Hanes 1998) for their closure. We anticipate that such an approach is appropriate for the flow of massive particles, where particle collision is indeed the major mechanism of intergranular interactions.

The large-scale sediment Reynolds stresses R_{xz}^{s} and R_{zz}^{s} result from the velocity and concentration fluctuations on a scale much larger than the grain size. Such large-scale fluctuations would not exist if the sediment was not in the turbulent flow of the fluid. Therefore, we shall propose a simple closure for the large-scale sediment Reynolds stress similar to the one-equation closure for the turbulent flow.

In the same way as the stresses, the flux of sediment fluctuation energy Q is taken to be the sum of small-scale Q_0- and large-scale Q_1-components:

$$Q = Q_0 + Q_1. \tag{2.29}$$

Finally, we take the rate of dissipation γ in equation (2.28) to be the collisional dissipation associated with the inelasticity of the particles.

Details of the modelling outlined above are provided in the following sections.

(ii) *Collisional granular flow theory*

The fundamental assumption of the present closure is that the particle normal stress τ^{s}_{zz} and the transport coefficients (e.g. the viscosity associated with the shear stress) are functions of sediment concentration $\bar{c}$, sediment properties, and sediment fluctuation energy K_{s}. Following Jenkins & Hanes (1998) for collisional granular flows, the transport coefficients in the constitutive relations for $\tau^{\mathrm{s}0}_{xz}$, $\tau^{\mathrm{s}0}_{zz}$, Q_0 and γ are obtained from the kinetic theory of dense gases (Chapman & Cowling 1970). The particle normal stress due to collision are taken to be

$$\tau^{\mathrm{s}0}_{zz} = -\tfrac{2}{3}\rho^{\mathrm{s}}\bar{c}(1+4G)K_{\mathrm{s}} + AE\frac{\partial \tilde{w}^{\mathrm{s}}}{\partial z}, \tag{2.30}$$

where $G \equiv \bar{c}g_0(\bar{c})$, with $g_0(\bar{c})$ the radial distribution function at contact for identical spheres. Torquato (1995) provides an accurate expression for this radial distribution function that is good for concentrations between 0.49, at which a phase transition between random and hexagonal packing is first possible, and the random close-packed concentration, $c^* = 0.635$, at which the mean distance between the edges' nearest neighbours is zero:

$$g_0(\bar{c}) = \begin{cases} \dfrac{2-\bar{c}}{2(1-\bar{c})^3}, & \bar{c} < 0.49, \\[2ex] \dfrac{2-0.49}{2(1-0.49)^3}\,\dfrac{0.64-0.49}{(0.64-\bar{c})^p}, & 0.49 \leqslant \bar{c} < 0.635, \end{cases} \tag{2.31}$$

where $p = 1$. The product AE in equation (2.30) is the sediment viscosity due to collisions. The particle collisional shear stress $\tau^{\mathrm{s}0}_{xz}$ is taken to be

$$\tau^{\mathrm{s}0}_{xz} = AE\frac{\partial \tilde{u}^{\mathrm{s}}}{\partial z}. \tag{2.32}$$

Based on the kinetic theory for collisional granular flow (Jenkins & Hanes 1998), we have

$$A = \frac{8d\rho^{\mathrm{s}}\bar{c}G(\frac{2}{3}K_{\mathrm{s}})^{1/2}}{5\pi^{1/2}} \quad \text{and} \quad E = 1 + \frac{\pi}{12}\left(1+\frac{5}{8G}\right)^2. \tag{2.33}$$

In a similar way, the flux of energy due to collision is taken to be

$$Q_0 = -\tfrac{5}{3}AM\frac{\partial K_{\mathrm{s}}}{\partial z}, \quad M = 1 + \frac{9\pi}{32}\left(1+\frac{5\pi}{12G}\right)^2. \tag{2.34}$$

Finally, based on the analysis of Jenkins & Savage (1983), the dissipation rate due to inelastic collision is

$$\gamma = \left(\frac{10A}{d^2} - 4\rho^{\mathrm{s}}\bar{c}G\frac{\partial \tilde{w}^{\mathrm{s}}}{\partial z}\right)(1-e)K_{\mathrm{s}}, \tag{2.35}$$

where e is the coefficient of restitution, taken here to be 0.8.

(iii) *Large-scale sediment stress*

We model the large-scale sediment Reynolds stresses R^{s}_{xz} and R^{s}_{zz} using an eddy viscosity. The shear stress is written as

$$R^{\mathrm{s}}_{xz} = \rho^{\mathrm{s}}\nu_{\mathrm{st}}\frac{\partial \tilde{u}^{\mathrm{s}}}{\partial z}, \tag{2.36}$$

and the normal stress as

$$R^{\mathrm{s}}_{zz} = -\tfrac{2}{3}\rho^{\mathrm{s}}\bar{c}K_{\mathrm{s}} + \tfrac{4}{3}\rho^{\mathrm{s}}\nu_{\mathrm{st}}\frac{\partial \tilde{w}^{\mathrm{s}}}{\partial z}. \tag{2.37}$$

The sediment viscosity ν_{st} is related to the sediment fluctuation energy through a sediment mixing length l_{s},

$$\nu_{\mathrm{st}} = C_{\mathrm{s}}\bar{c}l_{\mathrm{s}}\sqrt{K_{\mathrm{s}}}, \tag{2.38}$$

in which C_{s} is a numerical coefficient, taken to be 0.55 based on the value used in the one-equation turbulence model for clear fluid. The sediment mixing length needs to be specified. In sheet flow, the large-scale fluctuations in sediment velocity and concentration are primarily caused by the fluid flow turbulence. Therefore, we assume that the sediment mixing length can be related to turbulent fluid flow mixing length l_{f} through α,

$$l_{\mathrm{s}} = \alpha l_{\mathrm{f}}, \tag{2.39}$$

where the fluid turbulent mixing length is calculated from the fluid turbulent kinetic energy and its dissipation rate:

$$l_{\mathrm{f}} = 0.165\frac{k_{\mathrm{f}}^{3/2}}{\epsilon_{\mathrm{f}}}. \tag{2.40}$$

For massive particles with a long particle response time, $\alpha \approx 0$, the fluid turbulent eddies can not induce any sediment velocity fluctuations, and $l_{\mathrm{s}} \approx 0$. For fine particles with small particle response time, $\alpha \approx 1.0$, the fine particles follow the fluid turbulent eddies, and $l_{\mathrm{s}} \approx l_{\mathrm{f}}$.

Finally, the flux of energy due to large-scale sediment fluctuations is calculated as

$$Q_1 = -\rho^{\mathrm{s}}\frac{\nu_{\mathrm{st}}}{\sigma_{\mathrm{s}}}\frac{\partial K_{\mathrm{s}}}{\partial z}. \tag{2.41}$$

For simplicity, the numerical coefficient σ_{s} is taken to be 1.0.

(iv) *Modification at low concentration*

One of the fundamental assumptions of the kinetic theory of dense gases is that there are a significant number of collisions. Therefore, when the sediment concentration becomes very dilute, the validity of the collisional grain flow theory becomes questionable. In the upper portion of the sheet, away from the bed where the concentration becomes small, fluid turbulence becomes the major mechanism of sediment suspension. In addition, the fluid turbulence induces the transport of sediment momentum through the large-scale sediment Reynolds stress. Therefore, we anticipate that the lack of applicability of the collisional granular flow theory in very dilute conditions is of no great concern, provided that the small-scale stresses (τ^{s0}_{xz} and τ^{s0}_{zz})

of the collisional theory can be made to decay appropriately. Therefore, we introduce a damping parameter δ for the small-scale sediment stress defined in terms of the mean free path l_c of the sediment particles and the fluid turbulent mixing length l_f,

$$\delta \equiv \frac{l_f}{l_f + l_c}. \tag{2.42}$$

When the mean free path of collision becomes much larger than the fluid turbulent mixing length, the small-scale collisional transport is reduced through a diminishing δ.

In summary, based on (2.24), (2.32), (2.36) and (2.42), we rewrite the total sediment shear stress as

$$\tau_{xz}^{s} = \delta\tau_{xz}^{s0} + R_{xz}^{s} = (\delta AE + \rho^{s}\nu_{st})\frac{\partial\tilde{u}^{s}}{\partial z}, \tag{2.43}$$

and the total sediment normal stress as

$$\tau_{zz}^{s} = \delta\tau_{zz}^{s0} + R_{zz}^{s} = -\tfrac{2}{3}\rho^{s}\bar{c}[(1+4G)\delta + 1]K_s + (\delta AE + \tfrac{4}{3}\rho^{s}\nu_{st})\frac{\partial\tilde{w}^{s}}{\partial z}. \tag{2.44}$$

Similarly, the flux of sediment fluctuation energy is rewritten as

$$Q = Q_0 + Q_1 = -\left(\tfrac{5}{3}AM\delta + \rho^{s}\frac{\nu_{st}}{\sigma_s}\right)\frac{\partial K_s}{\partial z}. \tag{2.45}$$

(v) *The region of enduring contact*

The constitutive relations for particle collisions based on the kinetic theory of dense molecular gases have been successfully implemented to study problems of rapid granular flow at concentrations smaller than the random loose packing c_*. The primary reason for the close similarity between particle and molecular collisions is that they are of relatively short duration, compared with the time between collisions. However, for granular shearing flows at concentrations greater than c_*, particles are in enduring contact. Therefore, the analogy between the particles and molecules is no longer valid.

Here, we model the sediment transport above the stationary bed, where the concentration is near random close packing. Therefore, modifications to the collisional grain flow theory for the closure of particle stress are needed. The discrete particle simulations of Zhang & Campbell (1992) indicate that between the random close-packed concentration c^* and the random loose-packed concentration c_*, the granular material is in a transitional state between solid-like and fluid-like behaviour. Bocquet *et al.* (2001) carried out experiments on the Couette flow of grains in this regime and observed that the viscosity of the particle shear stress increased dramatically as the concentration approached c^*. They suggested that in the viscosity, the power p in equation (2.31) should be changed from 1.00 to 1.75. That is, in our numerical implementation, p is taken to be 1.00 when $\bar{c} < c_*$ and 1.75 when $\bar{c} \geqslant c_*$. Therefore, as far as the particle shear stress is concerned, the region involving enduring contacts is modelled by taking the granular material to be an extremely viscous fluid.

As the concentration increases above c_*, the collisional contribution to the particle normal stress diminishes, because the shearing of the particle phase that is the source of the collisional fluctuations becomes very small. However, in this range of concentration, the contribution to particle normal stress due to enduring contacts becomes important. Therefore, we further assume that the small-scale particle normal stress τ_{zz}^{s0} is the sum of the collisional normal stress τ_{zz}^{sc} and the normal stress τ_{zz}^{se} due to enduring contact:

$$\tau_{zz}^{s} = \tau_{zz}^{sc} + \tau_{zz}^{se}. \tag{2.46}$$

We model the collisional stress using equation (2.30), while for the normal stress due to enduring contact we adopt a Hertz contact relation. For a homogeneously packed, dry granular material consisting of identical spheres in Hertzian contact, the normal stress is (Jenkins *et al.* 1989)

$$\tau_{zz}^{se} = \frac{m}{\pi d^2} K \bar{c} \left(\frac{\Delta}{d} \right)^{3/2}, \tag{2.47}$$

where Δ is the average compressive volume strain, m is given in terms of the shear modulus μ_e and Poisson's ratio υ of the material of the particles

$$m = \frac{2}{9\sqrt{3}} \frac{\mu_e d^2}{1-\upsilon}, \tag{2.48}$$

and K is the average number of contacts per particle or coordination number. We do not solve for Δ, but assume that Δ/d can be related to the difference between the local average concentration and that of random loose-packing c_* by

$$\frac{\Delta}{d} = (\bar{c} - c_*)^{2\chi/3}, \tag{2.49}$$

in which χ is a coefficient. The numerical value of χ will be discussed in the following section. Then

$$\tau_{zz}^{se} = \begin{cases} 0, & \bar{c} < c_*, \\ \dfrac{m}{\pi d^2} K(\bar{c}) \bar{c} (\bar{c} - c_*)^{\chi}, & c_* \leqslant \bar{c} \leqslant c^*, \end{cases} \tag{2.50}$$

where the coordination number K is taken to be a function of concentration,

$$K(\bar{c}) = 3 + 3 \sin\left[\frac{\pi}{2} \left(2 \frac{\bar{c} - c_*}{c^* - c_*} - 1 \right) \right], \quad c_* \leqslant \bar{c} \leqslant c^*, \tag{2.51}$$

based on the best fit of the results from a discrete particle simulation (Duan Zhang 2001, personal communication). We note that, based on equation (2.50), the normal stress of enduring contact vanishes when the concentration is below c_*, where the average distance between particles is greater than zero. Moreover, unlike the relation provided by Johnson *et al.* (1990), the contact stress in the present model has a finite value at random close-packing.

(*d*) *Boundary conditions*

(i) *Boundary conditions at the stationary bed*

The bottom boundary condition of the sediment phase is applied at the interface between the porous stationary bed and the region of slow flow that involves enduring contacts. Within the porous stationary bed, the horizontal velocity, the vertical velocity, and the velocity fluctuations of the sediment vanish. Therefore we specify $\tilde{u}^{\mathrm{s}} = 0$, $\tilde{w}^{\mathrm{s}} = 0$ and $K_{\mathrm{s}} = 0$ at the stationary bed.

As the external shear stress changes, sediment particles can either be eroded from the bed and suspended in the flow or settle from the flow and accumulate on the bed. Therefore, the location of the bed changes as the external flow conditions change, and needs to be determined as a part of the solution. In order to shear or fluidize a granular material, the concentration must be at some value smaller than the random-close-packed concentration. We denote the concentration at which the bed fails by $\hat{c}$. In the present model, the failure concentration $\hat{c}$ is determined through the Coulomb failure criterion,

$$\tau^{\mathrm{s}}_{xz} = \tau^{\mathrm{s}}_{zz} \tan\phi, \tag{2.52}$$

where ϕ is the friction angle of the sediment. Upon substituting equations (2.46) and (2.50) into (2.52), we obtain

$$K\bar{c}(\bar{c} - c_*)^{\chi} = \frac{\pi d^2}{m}\left(\frac{\tau^{\mathrm{s}}_{xz}}{\tan\phi} - \tau^{\mathrm{sc}}_{zz}\right). \tag{2.53}$$

Because τ^{s}_{xz} and τ^{sc}_{zz} can be obtained independently from their proposed closures, the failure concentration $\hat{c}$ can be determined from the above nonlinear algebraic equation. Immediately above the stationary bed, the sediment particles are mobile and the sediment concentration there must equal $\hat{c}$. Hence, the bed location can also be determined. Because the magnitude of τ^{s}_{xz} varies with the external flow conditions, both the failure concentration and the bed location change with the external flow. Notice that, since the value of the calculated failure concentration $\hat{c}$ must be close to the random close-packed concentration c^*, this provides a way to determine a reasonable numerical value for χ. Based on numerical experiments for plastic particles implemented by Sumer *et al.* (1996), $\chi = 5.5$ gives a failure concentration of *ca.* 62%. Therefore, this value is adopted.

(ii) *Top boundary conditions*

In all of the laboratory experiments on sediment transport that we test the model against, the top boundary is any hydraulically smooth, rigid lid. Therefore, the boundary conditions for fluid velocity, k_{f} and ϵ_{f} are specified based on the log law of the wall (Rodi 1984), as commonly implemented for clear fluid flow.

Because the Neumann boundary conditions for the fluid pressure are specified on the lateral and lower boundary of the computational domain (see the next subsection for details), $\bar{P}^{\mathrm{f}} = 0$ is specified at the top boundary as the reference pressure for the flow.

In the present model, the top boundary of the sediment phase is considered to be at the point where the sediment concentration becomes smaller than a prescribed minimum concentration $c_{\min}$. Above this point, the sediment phase is considered to be negligible and is not calculated. The calculated results are insensitive to $c_{\min}$, as long as it is small enough. The value $c_{\min} = 5 \times 10^{-4}$ has been used in the present study.

At the top boundary of the sediment phase, the flow is dilute and the free-slip boundary conditions of sediment horizontal velocity $\tilde{u}^{\mathrm{s}}$ and fluctuation energy K_{s} are adopted. As the magnitude of the external flow changes, the point at which the calculated concentration equals to $c_{\min}$ also changes.

(iii) *Lateral boundary conditions: fluid pressure*

In the numerical solutions, the flow is driven by a horizontal pressure gradient. This is consistent with most of the laboratory U-tube experiments on sediment transport. However, in laboratory experiments that involve steady flows in a channel, the flow is driven by gravity. In this case, the gravity force in the fluid momentum equation is converted to an equivalent horizontal pressure gradient. Therefore, for a steady, gravity-driven flow with a given slope S or frictional velocity u_* and hydraulic radius r_{b}, the horizontal pressure gradient is prescribed as

$$\frac{1}{\rho^{\mathrm{f}}}\frac{\partial \bar{P}^{\mathrm{f}}}{\partial x} = gS = -\frac{u_*^2}{r_{\mathrm{b}}}. \tag{2.54}$$

On the other hand, for the uniform oscillatory flow in which the free stream velocity $u_0(t)$ oscillates as

$$u_0(t) = U_0 \sin\left(\frac{2\pi}{T}t\right), \tag{2.55}$$

where U_0 is the amplitude and T is the period of oscillation, the horizontal pressure gradient is prescribed as the acceleration of the free stream velocity:

$$\frac{1}{\rho^{\mathrm{f}}}\frac{\partial \bar{P}^{\mathrm{f}}}{\partial x} = -\frac{\mathrm{d}u_0(t)}{\mathrm{d}t} = -U_0\frac{2\pi}{T}\cos\left(\frac{2\pi}{T}t\right).$$

(iv) *A remark on the initial condition*

We do not attempt to describe the initiation of the sediment motion. Instead, we specify an artificial amount of sediment above the stationary bed with a given profile $\bar{c}_{\mathrm{ini}}(z)$, as the initial condition. We adopt a profile with maximum concentration c^* at the bed that decreases linearly to a concentration of 0.20 at about half the water depth. The fluid and sediment velocities are initially taken to be zero and, to speed the computation, the flow is calculated in an initial period 0 to T_0 with the vertical sediment velocity set equal to zero. The value of T_0 in each case is taken to be 10 times the turnover time $t_{\mathrm{L0}} = h/u_*$ of the largest eddy in the channel. In doing this, both the fluid and sediment phase horizontal velocity and fluctuation energy profiles become established. After $t = T_0$, the vertical motion of sediment is calculated based on the vertical sediment momentum equation. If this procedure is not implemented, it takes a very long time to reach the steady state, because the sediment settles quickly and need to be re-suspended as the fluid and sediment velocity and fluctuation energy profiles are established. In general, we need to calculate about 50 to 100 times the turnover time to obtain the steady-state solution.

3. Numerical implementation

The proposed two-phase equations (2.1)–(2.9), together with the sediment-phase fluctuation energy equation (2.28) and the fluid-phase energy and dissipation equations (2.17) and (2.23) are solved numerically with a finite-difference scheme. A staggered grid system is employed. That is, except for the vertical velocities of the fluid-phase $\tilde{w}^{\mathrm{f}}$ and sediment-phase $\tilde{w}^{\mathrm{s}}$ that are defined at the top-face of the grid, the rest of the variables are defined at the grid centre.

Because the flow is considered to be uniform in the x-direction, only the variations of the physical variables in the z-direction are of interest and solved for. The computational domain is discretized into $N+2$ grids with single ghost grids at the top and the bottom of the domain. In the present model, the flow is driven by the horizontal pressure gradient $\partial \bar{P}^{\mathrm{f}}/\partial x$. Therefore, two additional columns of ghost grids are implemented, in which the appropriate pressures are specified to achieve the desired pressure gradient.

A modified form of the two-step projection method (see, for example, Lin & Liu 1998) is implemented to solve the two-phase equations. At the beginning the computational cycle, we integrate the sediment phase mass and momentum equations in time using a predictor-corrector scheme. After obtaining all the sediment phase variables, $\bar{c}$, $\tilde{u}^{\mathrm{s}}$, $\tilde{w}^{\mathrm{s}}$ and K_{s} at a new time-step, the fluid phase mass and momentum equations are solved using a similar two-step projection method. At the end of the computational cycle, the fluid phase energy and dissipation equations are updated.

The time-step size Δt in the numerical model is adjusted dynamically at every time-step, based on several stability conditions. Because of the convection terms in both the fluid and sediment phase–momentum equations, the Courant condition

$$\Delta t \leqslant \frac{\eta_1 \Delta z}{\max(|\tilde{w}^{\mathrm{f}}|, |\tilde{w}^{\mathrm{s}}|)} \tag{3.1}$$

for the time-step size must be satisfied, where η_1 is a numerical coefficient, taken to be 0.3. The numerical stability of the diffusion term in the fluid and sediment phase momentum equations is guaranteed by the constraint

$$\Delta t \leqslant (\Delta z)^2 \left(\max\left[\nu_{\mathrm{ft}}, \left(\frac{\delta AE}{\rho^{\mathrm{s}} + \nu_{\mathrm{st}}} \right) \right] \right)^{-1}, \tag{3.2}$$

where $(\delta AE/\rho^{\mathrm{s}} + \nu_{\mathrm{st}})$ is the diffusion coefficient of the sediment momentum defined in (2.43).

Because of the interaction term in the momentum equations, additional constraints for the numerical stability of a two-phase system must be considered. Since the interaction term is a drag force, intuitively, the additional time-step constraint must be proportional to the particle response time t_{p}. A stability analysis of the momentum equation reveals that the size of the time-step for the drag force term is restricted by t_{p} divided by the specific gravity s. This restriction is taken to be

$$\Delta t \leqslant \eta_2 \frac{t_{\mathrm{p}}}{s}, \tag{3.3}$$

with $\eta_2 = 0.1$ being a conservative estimate. In every cycle, the time step Δt is determined by the minimum value of equations (3.1)–(3.3).

Further details of the numerical implementation and spatial discretizations are given by Hsu (2002).

4. Results

(*a*) *Steady flow*

The proposed sheet flow model is used to study the laboratory experiments of Sumer *et al.* (1996) for their sediment II (plastic particle, diameter $d = 2.6$ mm and specific gravity $s = 1.14$). The strength of the turbulent shear flow is characterized by the Shield parameter θ, defined in terms of the friction velocity u_* and the buoyant weight of a layer of grain material,

$$\theta \equiv \frac{\rho^{\mathrm{f}} u_*^2}{(\rho^{\mathrm{s}} - \rho^{\mathrm{f}}) g d}.$$

The concentration profiles and sediment velocity profiles are not measured for all cases of sediment II. However, the fluid velocity profiles for five cases of sediment II are reported. Therefore, we will first present the calculated results and describe the important physics of sheet flows for massive particles. We then present the comparisons of the fluid velocity with the available experimental data. Finally, we calculate some global parameters that are often employed for modelling large-scale river and coastal sediment transport.

We define a new vertical coordinate system z_{b} with its origin ($z_{\mathrm{b}} = 0$) at the initial undisturbed bed level of each case. Because an artificial sediment concentration profile $\bar{c}_{\mathrm{ini}}$ is prescribed as the initial condition, the initial bed level $z = z_0$ relative to the zero of the numerical computational domain can be calculated based on mass conservation:

$$z_0 = \frac{1}{c^*} \int_0^h \bar{c}_{\mathrm{ini}} \, \mathrm{d}z. \tag{4.1}$$

Therefore, the relation between the new vertical coordinate z_{b} and the original vertical coordinate z is $z_{\mathrm{b}} = z - z_0$.

Figure 1 presents calculated values of the concentration, the fluid and sediment velocity, the fluid turbulence and sediment fluctuation intensity, the shear stresses and the normal stresses for run 91 of Sumer *et al.* (sediment II, $\theta = 1.65$), in which the vertical coordinate is normalized by the grain diameter. The lowest vertical location shown in these plots is near the interface on which sediment particles first become mobile (the stationary bed). In the lowest portion of the sheet, within *ca.* 3 grain diameters ($\hat{c} > \bar{c} > c_*$), a highly concentrated, slow flow region with enduring contact appears with concentration slowly decreasing in the vertical direction. In the same region, both the fluid and sediment velocity are relatively weak. Such features are due to the contact stress and the high viscosity implemented in the model for the region of enduring contacts. We also observe that the fluid turbulence intensity almost vanishes in the region of enduring contact, due to slow flow and significant damping from the sediment.

Above the region of enduring contacts ($\bar{c} < c_*$), sediment concentration decreases much faster with z_{b}/d. However, there is clearly a region of *ca.* 6 grain diameters in thickness ($-3 < z_{\mathrm{b}}/d < 3$) that has a relatively uniform concentration of about 0.35. This 'shoulder' is consistent with the existence of a sheet. It also suggests that strong suspension mechanisms exist in this region. Referring to figure 1*c*, the shoulder also corresponds to a region of large sediment fluctuation energy. Above $z_{\mathrm{b}} \approx 5d$, sediment concentration decreases dramatically into a dilute region in which the fluid turbulent kinetic energy is greater than the sediment fluctuation energy. Notice that there are two peaks of the calculated intensity of sediment fluctuation energy in figure 1*c*. The peak located around $z_{\mathrm{b}}/d = -3$ corresponds to the region of high concentration, indicating strong particle collisions. On the other hand, a second weaker peak located around $z_{\mathrm{b}}/d = 10$ is due to strong fluid turbulent kinetic energy

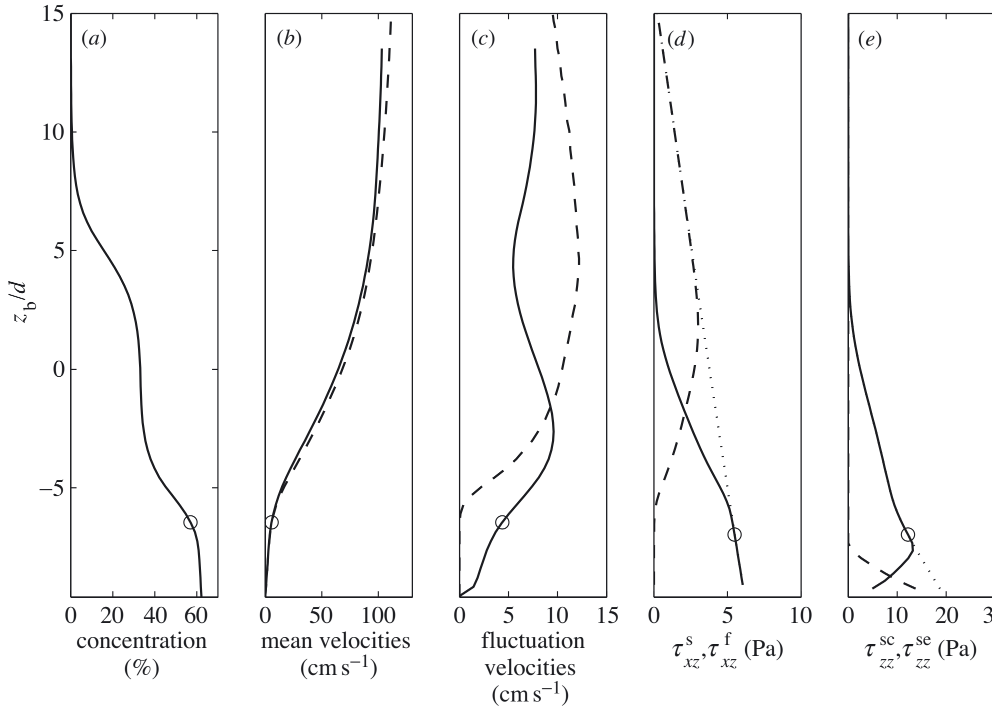

Figure 1. Results from the present model for run 91 of Sumer *et al.* (1996): (*a*) sediment concentration (%), with the failure concentration $\hat{c} = 62.1\%$; (*b*) – – – –, fluid velocity $\tilde{u}^{\mathrm{f}}$; ———, sediment velocity $\tilde{u}^{\mathrm{f}}$; (*c*) – – – –, fluid turbulence intensity $\sqrt{2k_{\mathrm{f}}}$; ———, intensity of sediment fluctuation energy $\sqrt{2K_{\mathrm{s}}}$; (*d*) – – – –, fluid shear stress τ^{f}_{xz}; ———, sediment shear stress τ^{s}_{xz}; $\cdots$, total shear stress $\tau^{\mathrm{f}}_{xz} + \tau^{\mathrm{s}}_{xz}$; (*e*) – – – –, sediment contact normal stress τ^{se}_{zz}; ———, sediment collisional normal stress τ^{sc}_{zz}; $\cdots$, total sediment normal stress $\tau^{\mathrm{se}}_{zz} + \tau^{\mathrm{sc}}_{zz}$. The '$\circ$' denotes the location corresponding to $c_* = 57\%$.

in the dilute region through the additional source term in the sediment fluctuation energy equation.

In figure 1*d*, due to the high sediment concentration within *ca.* 5 grain diameters above the stationary bed, the shear stress results mainly from the sediment phase. Above $z_{\mathrm{b}} \approx 0d$, the fluid (turbulent) shear stress becomes more significant than the sediment shear stress. The sum of the sediment and fluid stresses gives the expected linear distribution of the total shear stress in a fully developed flow. In figure 1*e*, the calculated sediment normal stresses due to enduring contact and collisions are shown. In the lower portion of the highly concentrated region of enduring contacts ($z_{\mathrm{b}}/d < -8.5$), the normal stress due to enduring contact is larger than the collisional stress. Notice that the gradient of the sediment normal stress is an important suspension mechanisms in the sediment vertical momentum equation.

Bagnold (1954) reported that the ratio between the particle shear stress and normal stress in the collisional region is about 0.32. The present model is used to test such a simple relation in inhomogeneous conditions. In figure 2*b*, the ratio between the calculated sediment shear stress τ^{s}_{xz} and normal stress τ^{s}_{zz} across the sheet of run 91 is presented. Overall, the ratio is not a constant. It varies from about 0.3 in the region of enduring contact to 0.5 in the region of intense collisions and decreases

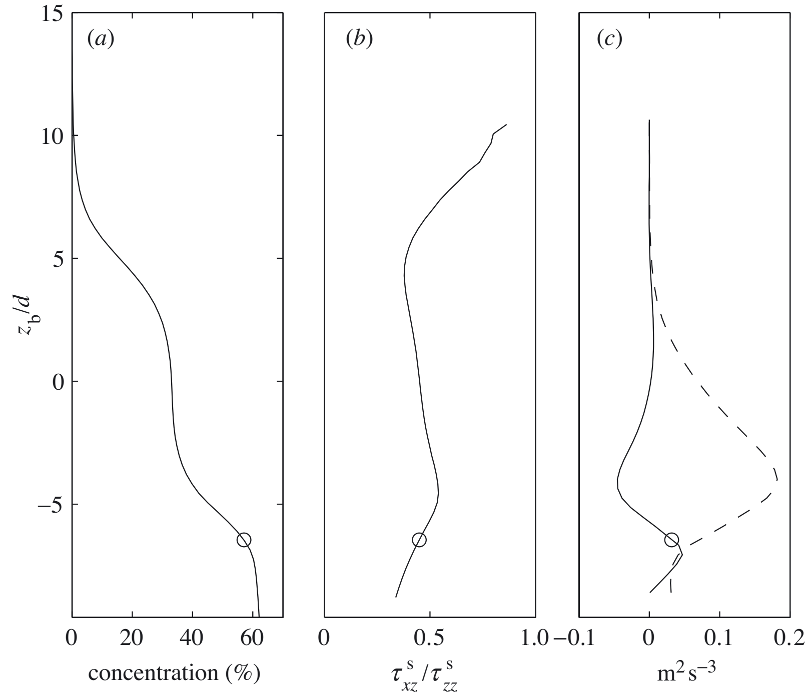

Figure 2. Results from the present model for run 91 of Sumer *et al.* (1996): (*a*) sediment concentration (%); (*b*) ratio between the sediment shear and normal stress τ^s_{xz}/τ^s_{zz}; (*c*) – – – –, production term, $1/\rho^s(\tau^s_{xz}(\partial\tilde{u}^s/\partial z)+\tau^s_{zz}(\partial\tilde{w}^s/\partial z))$; ———, diffusion term, $-1/\rho^s(\partial Q/\partial z)$, of the K_s equation. The '∘' denotes the location corresponding to $c_* = 57\%$.

to about 0.35 in the less-concentrated region. Additional insight can be obtained by examining the production and diffusion terms in the equation of the sediment fluctuation energy. In figure 2*c*, the production of K_s has its largest magnitude in the region around $z_b/d = -4$, where intensive collisions occur. Moreover, this is also the region of large transport. Because Bagnold's relation is based on homogeneous flow, one expects that his relation must become less accurate in a region of large transport. Indeed, at around $z_b/d = -4$, the ratio of shear to normal stress increases to about 0.5. In the less-concentrated region above $z_b/d = 0$, the magnitude of diffusion becomes much smaller and the shear-to-normal-stress ratio gradually approaches 0.3. Notice that, in the dilute region, the large-scale sediment Reynolds stress due to fluid turbulence becomes the major source of sediment stresses and the stress ratio increases again.

Sumer *et al.* (1996) reported five cases of measured fluid velocity profiles for sediment II. Although all of them have been used to test the present model, only three cases are shown here to illustrate important features. More comprehensive comparisons can be found in Hsu (2002). Figure 3 presents three comparisons of the calculated fluid velocity profiles with those measured by Sumer *et al.* (1996). In each case, the fluid velocity shown in the figures is normalized by the corresponding friction velocity $u_* = \sqrt{gr_bS}$, obtained from the measured energy slope S and hydraulic radius r_b. The corresponding calculated concentration profiles are shown in the left panel for reference. We remark here that because the experiment and the model

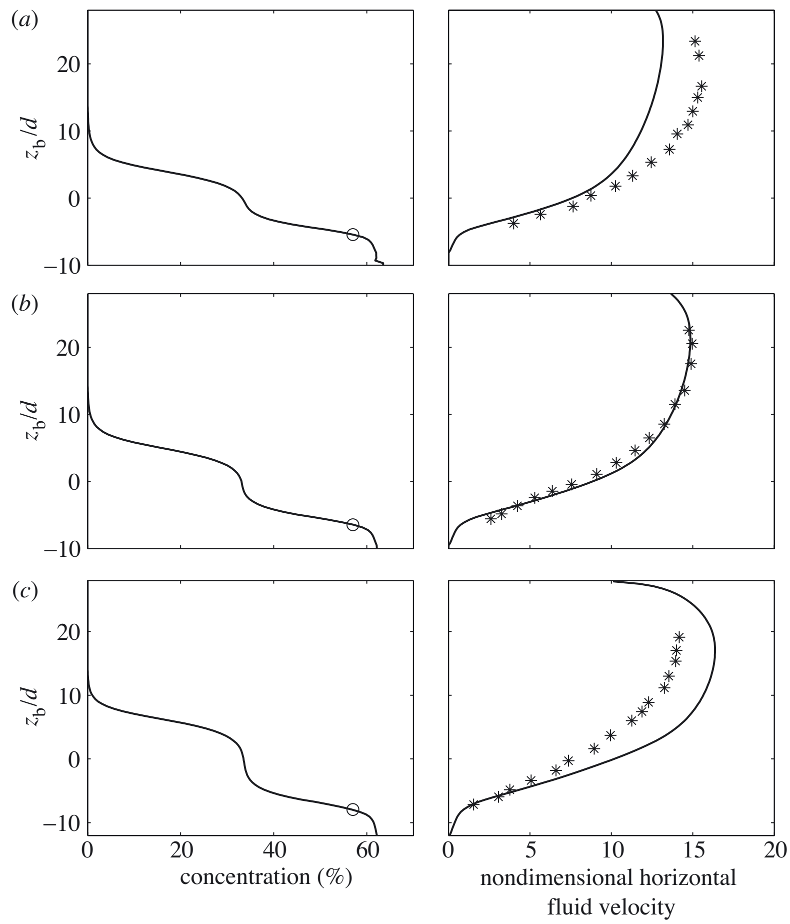

Figure 3. Comparison of the normalized fluid velocity profile, $\tilde{u}^{\mathrm{f}}/u_*$ (right panel), between the present model and the measurements of Sumer *et al.* (1996). The corresponding concentration profiles are shown in the left panel. (*a*) Run 82, $\theta = 1.37$ with the failure concentration $\hat{c} = 62.0\%$; (*b*) run 91, $\theta = 1.65$ with $\hat{c} = 62.1\%$; (*c*) run 99, $\theta = 2.30$ with $\hat{c} = 62.3\%$. $*$, measured data; ———, calculated results. The '$\circ$' denotes the location corresponding to $c_* = 57\%$.

begin with different initial amounts of total sediment, the location of the stationary bed in the final steady state for each case must be different. In the data reported by Sumer *et al.*, the origin of the vertical coordinate is defined at the stationary bed, which is obtained from visual observation or extrapolation of the measured fluid velocity profile. Moreover, because the measurement of the corresponding concentration profiles were not reported, it is difficult to perform a fair comparison between the calculated and the measured fluid velocity. In the present comparison, the stationary bed is located where the concentration is equal to the random loose-packed concentration, calculated from the model. Overall, the model tends to under-predict the fluid velocity for low Shields parameters and over-predict the fluid velocity for high Shields parameters.

The magnitude of the fluid velocity is closely related to the resistance of the bed and is usually represented by the roughness κ_{s}. As was suggested by Sumer *et al.*

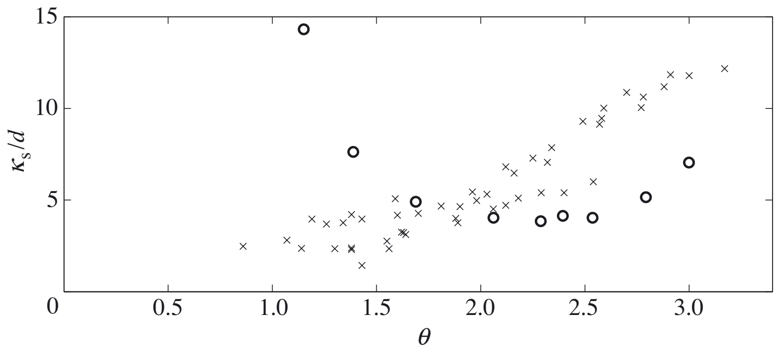

Figure 4. Comparison of roughness κ_s between $\times$, measured data, and $\circ$, results from the present model.

(1996), the roughness can be calculated based on the measured depth-averaged mean fluid velocity U by adopting Nikuradse's relation:

$$\frac{U}{u_*} = 2.46 \ln \frac{14.8 r_b}{\kappa_s}. \tag{4.2}$$

To further illustrate the predictions of the mean fluid velocity, figure 4 presents the comparison of roughness κ_s, calculated from equation (4.2), using the measured data and the results of the present model over a wide range of Shields parameters. Consistent with the under-prediction of fluid velocity in figure 3*a*, the present model significantly over-predicts the roughness at low Shields parameters. At high Shields parameters, although the model still under-predicts the magnitude of roughness, the increasing roughness with increasing Shields parameter of the measured data has been captured.

The reason that the model fails to predict an accurate fluid velocity at low Shields parameters may be related to the closure of fluid turbulence. That is, we anticipate that an under-prediction of mean fluid velocity may be due to an over-prediction of fluid turbulence. The closure of the additional dissipation mechanism in the energy equation (the last term in equation (2.17)) and the corresponding numerical coefficient $C_{3\epsilon}$ in the dissipation equation may not be appropriate for weak turbulence that involves high sediment concentration. Based on a direct numerical simulation of isotropic particle-laden turbulent flow, Squires & Eaton (1994) suggest that the value of $C_{3\epsilon}$ needs to be reduced as the concentration increases or the fluid turbulence decreases. A reduction of $C_{3\epsilon}$ increases the dissipation and, thus, reduces the energy and increases the mean flow velocity.

In modelling large-scale sediment transport, the sheet flow is usually not resolved and the hydraulic roughness becomes an important parameter that needs to be specified. For example, Grant & Madsen (1982) considered flow above a movable bed and found that the roughness was on the order of the thickness of the sheet flow layer. Therefore, the prediction of the sheet flow layer thickness δ_s is an important step towards better modelling of large-scale sediment transport.

However, the top of the sheet flow has not been well defined in the literature. In Sumer *et al.* (1996), the top of the sheet flow for large particles is obtained by visual observation, because direct measurements of the sediment concentration were not

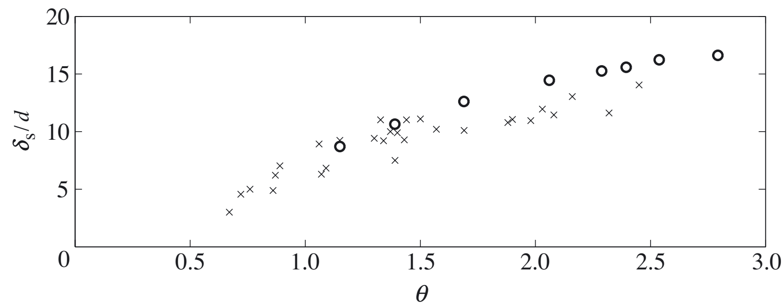

Figure 5. Comparison of sheet layer thickness δ_{s}. $\circ$, results from the present model; $\times$, visual observations by Sumer *et al.*

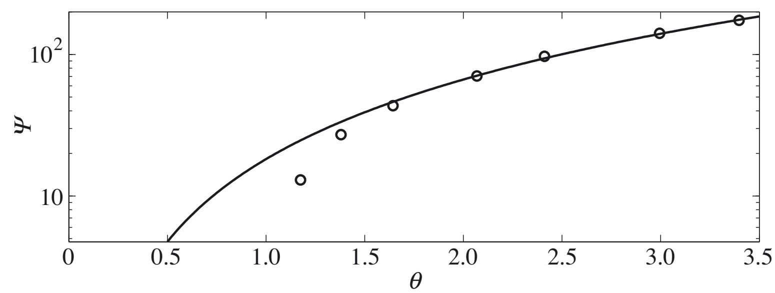

Figure 6. Non-dimensional total sediment transport rate $\Psi = q_{\mathrm{s}}/(d\sqrt{(s-1)gd})$ with respect to the Shields parameter. $\circ$, Results from the present model; ———, $\Psi = 20.0(\theta - 0.05)^{1.8}$.

made. It is reasonable to define the top of the sheet as the place where the concentration becomes small enough that the intergranular interactions are negligible. In this paper, we define the top of the sheet flow as the concentration of $\bar{c} = 0.08$, where the average distance between particles is one grain diameter (Torquato 1995). Then the sheet layer thickness $\delta_{\mathrm{sc}*}$ is defined as the distance from the random loose-packed concentration $c_* = 0.57$ to a concentration of 0.08. The calculated sheet layer thickness δ_{s}, normalized by the grain diameter are presented in figure 5 as a function of Shields parameter. The measured data of Sumer *et al.*, based on visual observations, are also shown in the figure. The calculated sheet layer thickness is quite consistent with the data of Sumer *et al.*

Finally, we examine the calculated total sediment transport rate as a function of the Shields parameter. The total sediment transport rate q_{s} is calculated by integrating the horizontal sediment flux $\bar{c}\tilde{u}^{\mathrm{s}}$ across the depth,

$$q_{\mathrm{s}} = \int_0^h \bar{c}\tilde{u}^{\mathrm{s}}\,\mathrm{d}z, \tag{4.3}$$

and is further non-dimensionalized by $\sqrt{(s-1)gd^3}$ and denoted by Ψ. Figure 6 presents calculated values of Ψ at various values of Shields parameter for sediment II. Notice that the total sediment transport rate considered here incorporates sediment transported throughout the water column. Hence, Ψ depends on the total water depth. For the data points shown in figure 6, the water depth is taken to be 20.0 cm, and significant sediment transport occurs only with the lower half of the depth. Using only the data points for Shields parameters greater than 1.5 (because the model tends to under-predicts the mean flow velocity and may not be accurate at low Shields parameters), we fit the calculated non-dimensional total sediment transport to

$$\Psi = C_0(\theta - \theta_c)^{\sigma}, \tag{4.4}$$

with the critical Shields parameter θ_c taken to be 0.05, and obtained $\sigma = 1.8$ and $C_0 = 20.0$. Since such global relations should also depend, at least, upon the ratio of the fall velocity to the friction velocity (Sumer *et al*. 1996), our results are not inconsistent with that reported by Ribberink (1998) in a review of laboratory and field experiments on steady sediment flows. Moreover, C_0 is expected to depend on the coefficient of restitution e, taken here to be 0.8.

(*b*) *Oscillatory flow*

To test the present model in the unsteady conditions, we study the U-tube experiments by Asano (1995) for uniform oscillatory flows. In order to be able to measure the sediment concentration and velocity using a high-speed video camera, Asano used relatively large plastic particles with a diameter $d = 4.17$ mm and specific gravity $s = 1.24$. Asano (1995) reports sediment concentrations and velocity profiles for his cases C-1, C-2 and C-4. Here, only a comparison with C-2 is shown. Comparisons with C-1 and C-4 can be found in Hsu (2002).

Figure 7 presents comparisons of concentration profiles at six different phases for case C-2 (oscillatory velocity amplitude $U_0 = 85.0\ \mathrm{cm\,s^{-1}}$, oscillatory period $T = 4.64$ s), while in figure 8 the corresponding comparisons of the sediment velocity profile at five different phases are shown. The calculated fluid velocity profiles are also shown in figure 8 for completeness. We note again that because the total amount of sediment in the experiment is not specified, the numerical model might have started with a different initial amount of sediment than the experiment, and we must shift the measured concentration profile in order to compare with the calculated results. Once we have determined the amount of shifting at the phase 0π for each test case, the same shift is used for the rest of the comparisons. There are larger discrepancies in the sediment velocity at the phase of $\frac{2}{3}\pi$. Notice also that there is significant scatter in the measured data, especially in the region of high concentration, suggesting uncertainties in the accuracy of the measurements due, for example, to the side-walls.

Figure 9 presents the sediment concentration time history at several elevations relative to the initial bed level for the case C-2. The corresponding time history of the free stream velocity is also shown. First, depending on the vertical locations relative to the initial bed, different behaviours of concentration time history can be observed. Below the initial bed level, the sediment concentration decreases as the free stream velocity increases. This is the pick-up layer (Ribberink & Al-Salem 1995). The pick-up layer is located below the initial bed level and extends to the stationary bed. When the free stream velocity increases, the concentration in the pick-up layer decreases as sediment is suspended. On the other hand, as the suspended sediment moves upward, the sediment concentration must increase in the region above the initial bed level. This region is called the upper-sheet flow layer (Ribberink & Al-Salem 1995). During the phase in which the free stream velocity decreases, sediment settles to the bed due to the excess of the gravity force over the suspension force. The sediment concentration in the upper-sheet flow layer decreases, while the concentration in the pick-up layer increases.

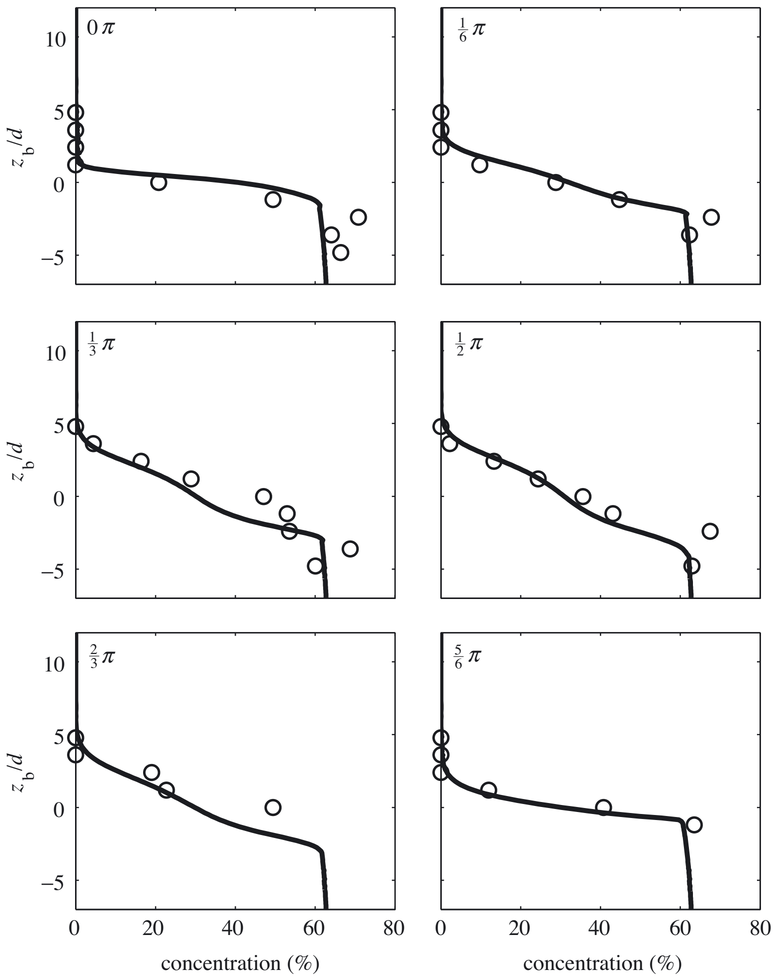

Figure 7. Comparison of concentration profiles between the results from the present model and the measured data for C-2 of Asano (1995) at six different phases. ———, present model results; ∘, measurements.

Using the present model, we calculate the time-averaged sediment transport rate over half a wave cycle

$$\langle q_{\mathrm{s}} \rangle_{\mathrm{w}} = \frac{2}{T} \int_0^{T/2} q_{\mathrm{s}} \, \mathrm{d}t,$$

where '$\langle \cdot \rangle_{\mathrm{w}}$' is the half-wave averaging operator, for uniform oscillatory flow under various amplitude of free stream velocity. Figure 10*a* presents the calculated $\langle q_{\mathrm{s}} \rangle_{\mathrm{w}}$ versus the third moment of the free stream velocity for half-wave $\langle u_0^3 \rangle_{\mathrm{w}}$ The calculated values $\langle q_{\mathrm{s}} \rangle_{\mathrm{w}}$ and $\langle u_0^3 \rangle_{\mathrm{w}}$ fit a linear relation reasonably. A similar trend has also been reported in experimental measurements (e.g. Asano 1995; Ribberink 1998). Moreover, in figure 10*b*, since the total bed shear stress can be calculated from the present model, we found that the best linear relation can be obtained by plotting $\langle q_{\mathrm{s}} \rangle_{\mathrm{w}}$, normalized by $\sqrt{(s-1)gd^3}$ and represented by Ψ_{w}, against the time-averaged 1.6th power of the Shields parameter. Notice that the predicted 1.6th power for the oscillatory flow is

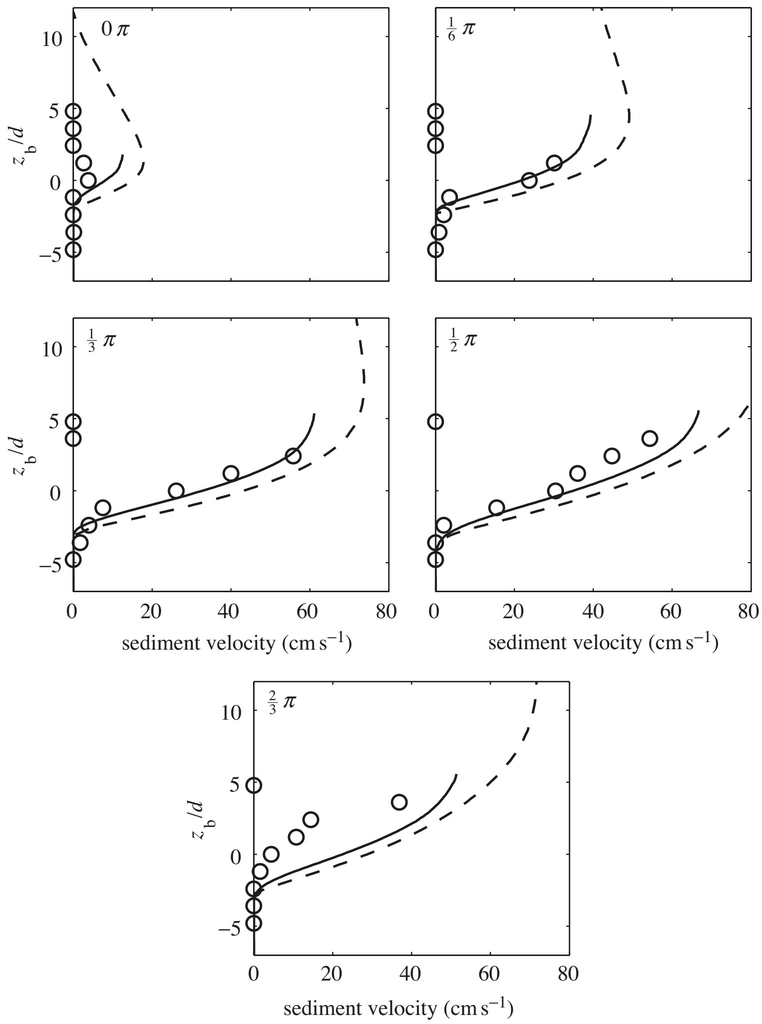

Figure 8. Comparison of sediment velocity profiles between the results from the present model and the measured data for C-2 of Asano (1995) at five different phases. ———, sediment velocity $\tilde{u}^{s}$ from the present model; ○, measured sediment velocity; – – – –, fluid velocity $\tilde{u}^{f}$ from the present model.

smaller than that predicted for the steady flow. We believe that this is because the sheet does not have enough time to become fully developed in the unsteady flow.

Although figure 10*a* implies the possibility of using the free stream velocity to estimate the sediment transport rate, we expect that such a method is not universal, especially for the highly unsteady flows (e.g. Drake & Calantoni 2001; Elgar *et al.* 2001) usually encountered in the near-shore environment. For most of the large-scale near-shore sediment transport models, the bed shear stress needs to be estimated, while, in a controlled experimental facility, a direct measurement of the bed shear stress is still not possible. The present computational model provides a new tool to obtain the information on free-stream velocity, bed shear stress and the corresponding sediment transport process simultaneously, in order to study their relationship.

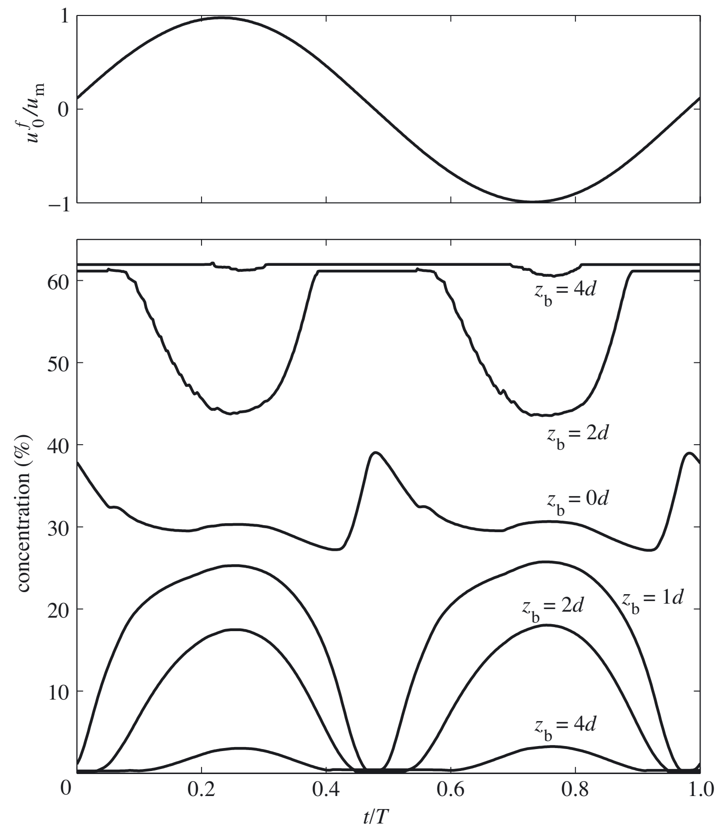

Figure 9. Time history of sediment concentration obtained from the present model at different locations relative to the initial bed for C-2 of Asano (1995). The top panel shows the corresponding time history of the free-stream velocity.

5. Concluding remarks

The two-phase model for sediment and fluid flow that we have introduced improves upon existing models in several ways. It incorporates turbulent suspension in the vertical momentum equation and includes dissipation and production due to particle–fluid interactions in the energy equations for the velocity fluctuations of both the turbulent fluid and the sediment. Comparisons with the experimental results on massive particles indicate that the predictions are generally good. However, future study on modelling the dissipation of the turbulent fluid energy in regions of high particle concentration is required to further improve the agreement between the experiments and theory.

We have attempted to provide a detailed model that is based upon plausible physics for the slow flow and failure of the bed. At least, the bed model permits us to describe erosion and deposition that occurs as the strength of the turbulent fluid flow changes with time. We anticipate that the bed model will be improved as more is learned about slow, concentrated flows of granular materials.

We have calculated several global quantities associated with the sheet flow that are of interest when modelling near-shore sediment transport processes. One of our goals

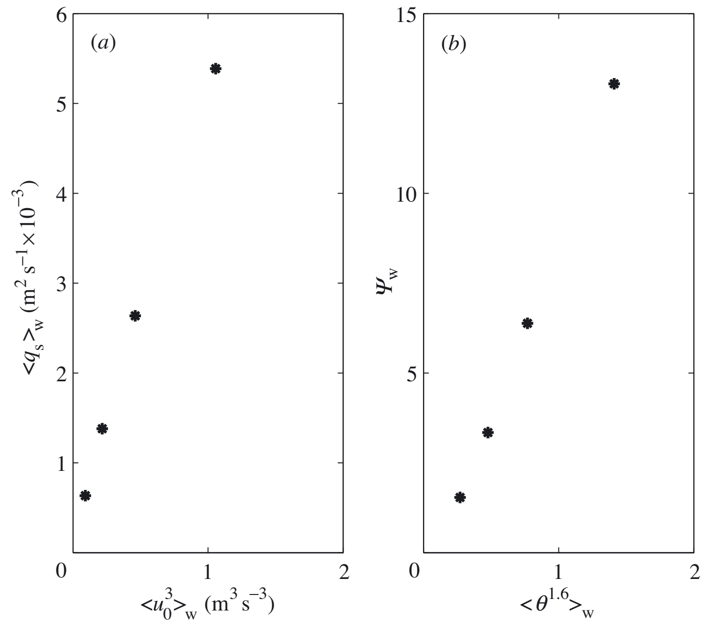

Figure 10. Time-averaged sediment transport rate over one half-wave cycle, $\langle q_s \rangle_w$, for various amplitude of free stream velocity. The oscillatory period is $T = 4.64$ s. Plastic particles have diameter $d = 4.17$ mm and specific gravity $s = 1.24$. (*a*) $\langle q_s \rangle_w$ versus the third power of free-stream velocity amplitude. (*b*) Normalized $\langle q_s \rangle_w$ versus the time-averaged 1.6th power of Shields parameter.

is to provide near-bed information to large-scale models that involve dilute sediment suspension and morphological changes occurring over widely different length and time-scales. For this, we must consider sand in water. The extension of the model to sand in water presents a challenge. In this case, the interaction between the particles is likely to be dominated, or at least strongly influenced, by the presence of the fluid, except, perhaps, in a region of high shear at concentrations slightly above random loose packed.

This research has been supported by NSF grants CTS-0000675 and OCE-0095834 and NASA grant NAG3-2353 to Cornell University.

References

Asano, T. 1990 Two-phase flow model on oscillatory sheet flow. In *Proc. 22nd Int. Conf. Coastal Engineering*, pp. 2372–2384. Reston, VA: American Society of Civil Engineers.

Asano, T. 1995 Sediment transport under sheet-flow conditions. *J. Wtrwy Port Coastal Ocean Engng* **121**(5), 1–8.

Bagnold, R. A. 1954 Experiments on a gravity-free dispersion of large solid spheres in a Newtonian fluid under shear. *Proc. R. Soc. Lond.* A **225**, 49–63.

Bocquet, L., Losert, W., Schalk, D., Lubensky, T. C. & Gollub, J. P. 2001 Granular shear flow dynamics and forces: experiment and continuum theory. *Phys. Rev.* E **65**, 011307.

Chapman, S. & Cowling, T. G. 1970 *The mathematical theory of non-uniform gases*, 3rd edn. Cambridge University Press.

Dong, P. & Zhang, K. 1999 Two-phase flow modeling of sediment motions in oscillatory sheet flow. *Coastal Engng* **36**, 87–109.

Drake, T. G. & Calantoni, J. 2001 Discrete particle model for sheet flow sediment transport in the nearshore. *J. Geophys. Res.* **106**, 19 859–19 868.

Drew, D. A. 1976 Production and dissipation of energy in the turbulent flow of a particle–fluid mixture, with some results on drag reduction. *J. Appl. Mech.* **43**, 543–547.

Drew, D. A. 1983 Mathematical modeling of two-phase flow. *A. Rev. Fluid Mech.* **15**, 261–291.

Elgar, S., Gallagher, E. L. & Guza, R. T. 2001 Nearshore sandbar migration. *J. Geophys. Res.* **106**, 11623–11627.

Elghobashi, S. E. & Abou-Arab, T. W. 1983 A two-equation turbulence model for two-phase flows. *Phys. Fluids* **26**, 931–938.

Favre, A. 1965 Equations des gaz turbulent compressible. *J. Méc.* **4**, 361–390.

Gore, R. A. & Crowe, C. T. 1989 Effect of particle size on modulating turbulent intensity. *Int. J. Multiphase Flow* **15**, 279–285.

Grant, W. D. & Madsen, O. S. 1982 Movable bed roughness in unsteady oscillatory flow. *J. Geophys. Res.* **87**, 469–481.

Greimann, B. P. & Holly, F. M. 2001 Two-phase flow analysis of concentration profiles. *J. Hydraul. Engng* **127**, 753–762.

Hanes, D. M. & Bowen, A. J. 1985 A granular-fluid model for steady intense bed-load transport. *J. Geophys. Res.* **90**, 9149–9158.

Hsu, T.-J. 2002 A two-phase flow approach for sediment transport. PhD thesis, University, Ithaca, NY, USA.

Hsu, T.-J., Jenkins, J. T. & Liu, P. L.-F. 2003 On two-phase sediment transport: dilute flow. *J. Geophys. Res.* **108**, 3057. (DOI: 10.1029/2001JC001276.)

Hwang, G.-J. & Shen, H. H. 1993 Fluctuation energy equations for turbulent fluid-solid flows. *Int. J. Multiphase Flow* **19**, 887–895.

Jenkins, J. T. & Askari, E. 1991 Boundary conditions for rapid antigranulocytes flows—phase interface. *J. Fluid Mech.* **223**, 497–508.

Jenkins, J. T. & Hanes, D. M. 1998 Collisional sheet flows of sediment driven by a turbulent fluid. *J. Fluid Mech.* **370**, 29–52.

Jenkins, J. T. & Savage, S. B. 1983 A theory for the rapid flow of identical, smooth, nearly elastic particles. *J. Fluid Mech.* **370**, 29–52.

Jenkins, J. T., Cundall, P. A. & Ishibashi, I. 1989 Micromechanics modeling of granular material. In *Powders and grains* (ed. J. Biarez & R. Gourves), pp. 257–264. Rotterdam: Balkema.

Johnson, P. C., Nott, P. & Jackson, R. 1990 Frictional-collisional equations of motion for particulate flows and their application to chute. *J. Fluid Mech.* **210**, 501–535.

Kobayashi, N. & Seo, S. N. 1985 Fluid sediment interaction over a plane bed. *J. Hydraul. Engng* **111**, 903–921.

Lin, P. & Liu, P. L.-F. 1998 A numerical study of breaking waves in the surf zone. *J. Fluid Mech.* **359**, 239–264.

McTigue, D. F. 1981 Mixture theory for suspended sediment transport. *J. Hydraul. Div. ASCE* **107**, 659–673.

Nott, P. R. & Brady, J. F. 1994 Pressure-driven flow of suspension: simulation and theory. *J. Fluid Mech.* **275**, 157–199.

Onoda, G. Y. & Liniger, E. G. 1990 Random loose packing of uniform spheres and the dilatancy onset. *Phys. Rev. Lett.* **64**, 2727–2730.

Ribberink, J. S. 1998 Bed-load transport for steady flows and unsteady oscillatory flows. *Coastal Engng* **34**, 59–82.

Ribberink, J. S. & Al-Salem, A. A. 1995 Sheet flow and suspension of sand in oscillatory boundary layers. *Coastal Engng* **25**, 205–225.

Richardson, J. F. & Zaki, W. N. 1954 Sedimentation and fluidization. Part 1. *Trans. IChE* **32**, 35–53.

Rodi, W. 1984 *Turbulence models and their application in hydraulics: a state of the art review.* Delft: IAHR.

Squires, K. D. & Eaton, J. K. 1994 Effect of selective modification of turbulence on two-equation models for particle-laden turbulent flows. *J. Fluids Engng* A **116**, 778–784.

Sumer, B. M., Kozakiewicz, A., Fredsoe, J. & Deigaard, R. 1996 Velocity and concentration profiles in sheet-flow layer of movable bed. *J. Hydraul. Engng* **122**, 549–558.

Torquato, S. 1995 Nearest-neighbor statistics for packings of hard spheres and disks. *Phys. Rev.* E **51**, 3170–3182.

Wilson, K. C. 1987 Analysis of bed-load motion in high shear stress. *J. Hydraul. Engng* **113**, 97–103.

Zhang, Y. & Campbell, C. S. 1992 The interface between fluid-like and solid-like behavior in two-dimensional granular flows. *J. Fluid Mech.* **237**, 541–568.

As this paper exceeds the maximum length normally permitted,
the authors have agreed to contribute to production costs.